

Neural Point Light Fields

Julian Ost¹ Issam Laradji² Alejandro Newell³ Yuval Bahat³ Felix Heide^{1,3}
¹Algolux ²McGill ³Princeton University

Abstract

We introduce *Neural Point Light Fields* that represent scenes implicitly with a light field living on a sparse point cloud. Combining differentiable volume rendering with learned implicit density representations has made it possible to synthesize photo-realistic images for novel views of small scenes. As neural volumetric rendering methods require dense sampling of the underlying functional scene representation, at hundreds of samples along a ray cast through the volume, they are fundamentally limited to small scenes with the same objects projected to hundreds of training views. Promoting sparse point clouds to neural implicit light fields allows us to represent large scenes effectively with only a single implicit sampling operation per ray. These point light fields are as a function of the ray direction, and local point feature neighborhood, allowing us to interpolate the light field conditioned training images without dense object coverage and parallax. We assess the proposed method for novel view synthesis on large driving scenarios, where we synthesize realistic unseen views that existing implicit approaches fail to represent. We validate that *Neural Point Light Fields* make it possible to predict videos along unseen trajectories previously only feasible to generate by explicitly modeling the scene.

1. Introduction

Learning implicit volumetric scene representations has made it possible to synthesize photo-realistic images of single scenes [22, 26, 29, 41]. The most successful methods combine a conventional volumetric rendering approach with a coordinate-based neural network that predicts density and radiance [26]. As such, instead of explicitly storing density and radiance in a high-dimensional 5D volume, these methods represent this volume as a learned function, that can be further decomposed into radiance and illumination [53, 42, 7]. Although the implicit volumetric representation is highly memory-efficient and differentiable, it also fundamentally requires sampling the volume, that is evaluating the coordinate-based network, hundreds of times for each ray for a given pixel. This mandates long training and small volumetric support inside the volume.

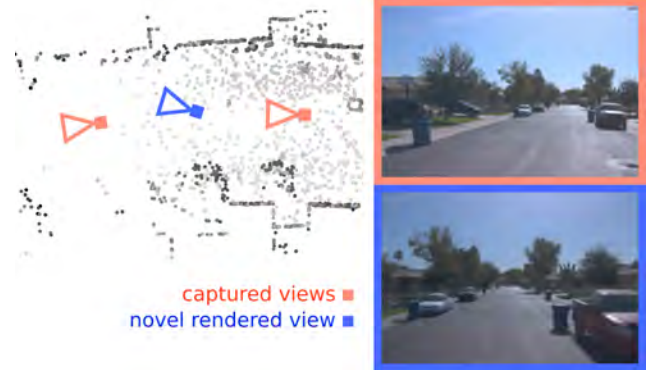


Figure 1: Neural Point Light Fields encode a local light field on a point cloud. An image is rendered for each camera ray and the local encoding of the light field on relevant points.

To tackle these challenges, hybrid representations [15, 21, 17] are used to embed or “bake” local implicit functions on explicit sparse proxy representations such as coarse voxel grids, point clouds or meshes to enable faster rendering by ignoring empty space. While this approach drastically improves rendering speed at test time, it still requires volumetric sampling during training. This is because the scene geometry must be learned during the training process. These methods share the limitations of volumetric approaches during training and, as such, have also been limited to small scenes that are costly to train. Learning representations for large outdoor scenes is an open challenge.

Unfortunately, approaches that are free of implicit representations do not yet offer an alternative. Specifically, explicitly storing features on proxy geometry [36, 35, 19] has not been able to achieve the same quality as volumetric methods when interpolating a view without a nearby training sample. Existing formulations utilize geometry as a projection canvas combined with features extracted from target views, and therefore require a large number of input images near the target view.

In this work, we depart from volumetric models and introduce *Neural Point Light Fields*, a local implicit representation that encodes a light field on a point cloud. The proposed representation supports novel view synthesis in large outdoor scenes without strong parallax needed as in

volumetric methods. Although recent automotive depth estimation networks make it possible to estimate dense depth point clouds from video data, we assume measured lidar point clouds as input to our method, especially as lidar data is readily available in most outdoor vehicle datasets [44, 12] and recent smartphone cellphones. Although sparse, the lidar geometry provides enough cues to encode a local light field on the point cloud. Instead of a 5D volumetric radiance function, or a conventional 4D light field [20], we propose to formulate a light field only depending on the two dimensional ray direction and a one dimensional index pointing to a point cloud feature, an implicit 3D representation. This formulation makes it possible to evaluate a *single* radiance prediction per ray. Traditionally, view-dependent effects captured in light fields have been analyzed by presenting epipolar plane images [6] (EPI), which capture 2D slices of a light field that interpolating between two extremal views. In Fig. 2 we present EPIs rendered from trained Neural Point Light Fields.

We extract features for each point with a learned feature extractor on point cloud projections [13]. For a given camera pose, we shoot rays for each pixel and select a set of close points inside the point cloud. The features from these selected points are then weighted by passing the points relative position to the ray and features through an attention module, resulting in a single ray feature code. The color for each ray is then reconstructed by an implicit light field representation conditioned by this feature code. To enforce local feature variations per point we store the point features after that first training stage and refine the point features in a second training stage. We assess the proposed method on a large-scale automotive driving dataset [44] and demonstrate novel view synthesis along unseen trajectories with quality unseen before.

Specifically, we make the following contributions

- We introduce Neural Point Light Fields, a representation that implicitly encodes features in a point cloud, allowing for a single radiance evaluation per ray.
- The proposed method lifts the restrictions of volumetric neural scene representations by exploiting sparse geometry available in estimated or captured point clouds.
- We validate the proposed method on novel video synthesis tasks for large-scale driving scenes, where we demonstrate that the proposed method is capable of generating realistic novel views along trajectories that existing implicit scene representation methods fail for.

We will release all source code and trained models to make the proposed model fully reproducible.

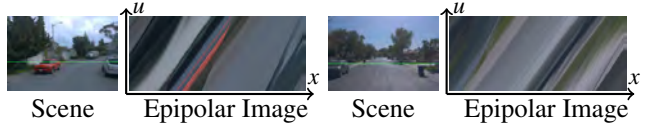


Figure 2: Epipolar Plane Images (EPI) rendered from a Neural Point Light Field. Our light field representation is only trained on a set of images from a monocular camera on a single trajectory through the scene. Despite having sparse views, we are able to synthesize realistic view extrapolations and accurately capture view-dependent light field effects.

Scope Even though existing automotive datasets include data from multiple cameras, lidar and radar sensors, we focus on this work to learn from a single camera with a single trajectory per scene, and without highly dynamic scene motion. We note that training on multiple camera views is not straightforward as camera poses, exposure and tone-mapping differences have to be accounted for. Incorporating multiple cameras and dynamic object suppression into the proposed method could be exciting future directions.

2. Related Work

Novel View Synthesis. Synthesizing novel views from a set of unstructured images of a scene is a long standing problem in computer vision and graphics. Early work on image-based rendering introduces light fields [20] as a 4D parametrization of light rays and their respective radiance in a scene. Light fields are derived by considering a convex subspace of the 5D plenoptic function [1] that parametrized a ray by a point in space and a direction. Conventional light field rendering, i.e., interpolation of novel views, required a large set of densely sampled views of the light field as traditional optimization methods [49, 50] handle only small parallax changes between the interpolated and measured view. Recently, methods relying on deep learning [25] introduced a method to recover the light field using from plane sweep volumes using 3D convolutional neural networks.

An orthogonal line of work investigates the reconstruction of explicit 3D models from a set of images. By optimizing the reprojection error between features found in all images, multi-view reconstruction methods are capable of reconstructing the underlying scene geometry and camera poses [2, 38]. These methods are able to reconstruct large scenes but also require many images to achieve high quality, and, in contrast to image-based rendering methods, they struggle to synthesize photorealistic novel views.

Neural Scene Representations. A large body of work has emerged that explores learned representations in scene reconstruction pipelines. These neural rendering approaches are able to generate photo-realistic novel views [22, 29] and they are capable of reconstructing high-quality scene geometry. Existing methods rely on explicit, implicit,

or hybrid representations of the scene. Explicit methods recover proxy geometry of the scene that hosts texture or radiance features, such as meshes [46], multi-planes [10, 23, 25, 43, 54], voxels [40] or points [3, 33]. Instead of having to recover geometry and appearance jointly, these methods can focus on the recovery of image detail. However, at the same time, relying on explicit proxy geometry also limits the achievable image quality. To overcome the reliance on such geometry, researchers explored implicit representations that represent scenes using coordinate-based networks. The most successful methods [26] represent volumetric density using such a coordinate-network. However, while achieving photo-realistic quality for diverse tasks [24, 31, 51, 42, 39, 28, 30], this comes at the cost of expensive training and testing. The lack of explicit geometric knowledge requires evaluating the implicit network densely in the volume with the majority of samples located in empty space that do not contribute to the rendered pixel color. Extensions [11] have tackled this issue at test time evaluation by either predicting the sampling regions [27, 5] or explicitly extracting proxy geometry [21] after training. DS-NeRF [8] uses 3D keypoints reconstructed from COLMAP on a scene to supervise the opacity prediction with those sparse keypoints, which speed up training. Neural Sparse Voxel Fields (NSVF) [21] are a hybrid representation that stores implicit functions in a voxel grid. All of these methods *struggle with large scale outdoor scenes or scenes with very few view observations*. In contrast, the proposed approach allows for large outdoor scenes from a sparse set of observations by introducing a light field parameterization on sparse scene geometry.

Multi-View Structure Reconstruction. Reconstructing geometry such as point clouds or meshes from images [38, 37] can guide the training of implicit scene representations [8] or offer a scaffold for learned features [36, 19]. Riegler and Koltun [36, 35] propose such geometric scaffolds living on MVS-meshes. Kopanas et al. [19] showed that optimizing the point location from an initial point cloud together with their novel view synthesis pipeline can compensate for the errors during reconstruction from MVS. These methods and similar [4] point based approaches use point clouds as a geometric proxy while following a strict rendering and projection approach. In contrast, we propose a method that uses features not only as a projection and aggregation surface but are encoded from a 3D point cloud and that does not require any input images during test time.

Encoding features directly on a point clouds has been extensively explored [34] for diverse tasks. Recent work revisited the use of multi-view projections of a point cloud for classification tasks [13, 14] similar to the presented reconstructions from point clouds, but not using image features. Their method is robust to occlusions [14] and achieves state-of-the-art results on their selected downstream tasks. In-

stead of solving a classification or segmentation task, we show that multi-view point cloud encoding can deliver rich local point features for reconstruction of novel views.

3. Point Light Fields

In this section, we introduce Point Light Fields. A Point Light Field encodes the light field of a scene on sparse point clouds. Assuming a camera-lidar sensor setup typical in robotic and automotive contexts [12], at time step i , the proposed method learns an RGB frame \mathcal{I}_i as input and the corresponding point cloud capture \mathcal{P}_i . To learn a light field implicitly embedded on the point clouds corresponding to a video sequence, we devise three steps: an encoding step, a latent feature aggregation, and a point-conditioned light field prediction, all of which we describe in the following.

3.1. Per-point Feature Encoding

We first produce a feature embedding for each point in the point cloud. To do this, we follow the simple strategy presented by Goyal et al. [13]. The input point cloud is projected onto six planes producing sparse depth images. These images are each fed directly into a convolutional network. We use the initial layers of a vanilla ResNet18 [16] to extract per-pixel features at one-quarter the input resolution. For a given point x_k , we retrieve the corresponding feature vector at its projected location in each of the six views. These are concatenated together to produce the final feature encoding $l_k \in \mathbb{R}^{6 \times 128}$.

We find it sufficient to normalize input point clouds to a canonical cube bounded by $[-1, 1]$ and use the 6 sides of the cube as projection planes. This works robustly even given the complexity of in-the-wild large-scale scenes. We perform ablations comparing features encoded using this strategy against alternative point-based models such as PointNet [34], see Supplementary Material.

The learned per-point features l_k do not depend on any image data and can be trained end-to-end with the full light field rendering. We can introduce augmentations such that the model does not overfit to a particular arrangement of points. This includes sampling different subsets of points from the full captured point cloud, and using point cloud captures from nearby time steps.

3.2. Light Field Feature Interpolation

Given a set of points $\mathcal{P}_i = \{x_0, \dots, x_N\}_i$ with $x_k \in \mathbb{R}^3$, their encoded features $l_k \in \mathbb{R}^{6 \times 128}$, and a camera view C_i , defined by its intrinsic K , extrinsic E_i and sensor dimensions W and H , we aggregate the relevant features that reconstruct the local light field around each ray. For all $W \times H$ pixels from C_i we cast a set of rays \mathcal{R}_i into the scene using a pinhole camera model. Each $r_j \in \mathcal{R}$ is defined by its origin o_j and viewing direction d_j .

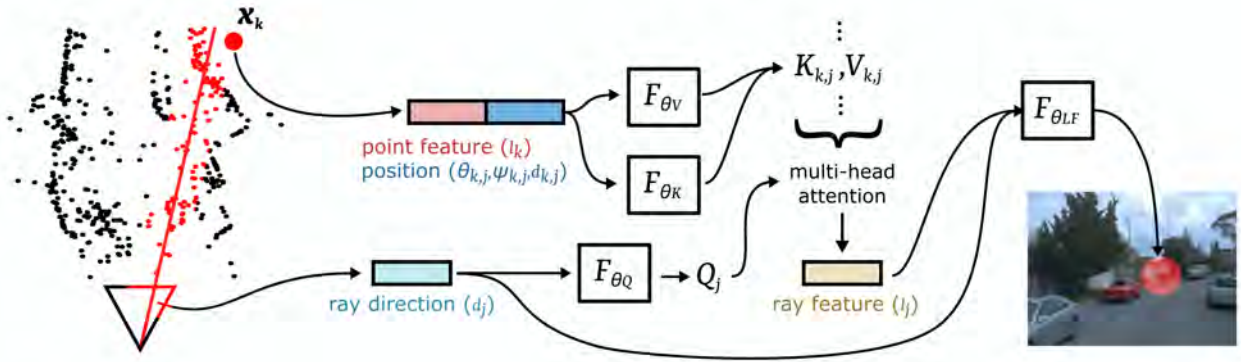


Figure 3: Neural Point Light Field Rendering Pipeline. For each ray r_j a set of K closest points is selected from a point cloud of the scene. From each point x_k a latent encoding l_k and the relative location with respect to r_j predict a key and value vector. The most relevant point features are aggregated for the ray with a multi-head attention module using the encoded ray direction d_j to form the query vector. A light field function $F_{\theta_{LF}}$ computes the ray color given the ray feature l_j and ray direction d_j .

Local Point Selection. The local point cloud encoding can explain the scene properties at their sparse locations. To explicitly represent high-frequency light field detail from all views a dense descriptor would be necessary. Instead, we implicitly interpolate a representation descriptor for each ray. The work of DeVries et al. [9] shows that the interpolation of local latent descriptors allows for implicit scene representations of large indoor scenes. Unlike their regular grid structure, we want to leverage the information given through the geometric properties of the point cloud. We assume that point features l_k hold enough information not only to represent the light field at their exact location but in their neighbourhood. We aggregate a descriptor for each ray r_j from a relevant set of sparse points. To this end, we select a set of K points $P_{j,i} \subset \mathcal{P}_i$ inside the viewing frustum of the camera C_i , with the smallest orthogonal distance $d_{k,j}$ between the points and the ray, as formulated in Eq. 2.

$$\cos(\varphi_{k,j}) = d_{j,i} \cdot \left(\frac{x_{k,i} - o_{j,i}}{\|x_{k,i} - o_{j,i}\|} \right) \quad (1)$$

$$d_{k,j} = \sin(\varphi_{k,j}) \cdot (x_{k,i} - o_{j,i}) \quad (2)$$

with $\sin(\varphi_{k,j}) = \sqrt{1 - \cos^2(\varphi_{k,j})}$

The ray origin $o_{j,i}$, the normalized ray direction $d_{j,i}$, and the point $x_{k,i}$ are all given in a local reference frame centered in the captured P_i . A light field descriptor is then generated for each ray considering all encoded features on the points in $P_{j,i}$.

Ray-centric Point Encoding. There are several immediate choices for the point embeddings of $P_{j,i}$, including average pooling, max pooling or a linear weighting by the distance $d_{j,k}$ of the selected K point features. However, these interpolation methods are ambiguous, thus can deliver the same descriptor for various rays and features on the same set of closest points $P_{j,i}$. In order to ensure a consistent and unique description for each ray from the same set, $P_{j,i}$ must consider an unambiguous relative position of all points with re-

spect to that ray, with coherence across different time steps i of the same scene.

As illustrated in Fig. 4 and formalized in Eq. 2, 5 and 4, we parameterize a close point by the angle $\theta_{k,j}$ between x_k and the ray d_j , the orthogonal distance between the point, and ray and the angle ψ that is defined as the radial coordinate of a projected x_k onto a plane defined through a projection of the global Y -axis and it's cross product with the ray direction d_j in Eq. 3.

$$\begin{bmatrix} x \\ y \end{bmatrix}_{k,j,proj} = \begin{bmatrix} y_j^T \\ (d_j \times y_j)^T \end{bmatrix} x_k, \quad (3)$$

$$\text{with } y_j = \frac{Y - (Y \cdot d_j) d_j}{\|Y - (Y \cdot d_j) d_j\|} \text{ and } y \in \mathbb{R}^3,$$

$$\psi_{k,j} = \arctan \frac{x_{k,j,proj}}{y_{k,j,proj}}. \quad (4)$$

Note that $\theta_{j,k}$ is computed between the global point x_k and d_j in world coordinates, independent of the position, and therefore different from the local $\varphi_{j,k}$, that computes the distance, that is

$$\theta_{k,j} = \arccos \left(d_{j,i} \cdot \frac{x_k}{\|x_k\|} \right). \quad (5)$$

Ray Feature Attention. Instead of applying an arbitrary chosen weighting for the ray features, we propose a learned multi-head attention module presented in Fig. 5 to compute the ray feature vector l_j . We propose a variant of the multi-head attention module presented by Vaswani et al. [47]. In the experimental Sec. 4 we compare the chosen attention based weighting with other linear interpolation schemes.

$$\gamma(s) = [\dots, \sin(2^t \pi s), \cos(2^t \pi s), \dots] \text{ with } t = 0, \dots, T \quad (6)$$

$$v_{k,j} = (l_k \oplus \gamma(\theta_{k,j}) \oplus \gamma(\psi_{k,j}) \oplus \gamma(d_{k,j})) \quad (7)$$

The two angular distances $\theta_{k,j}$ and $\psi_{k,j}$, as well as $d_{k,j}$ are transformed using the positional encoding in Eq. 6 with

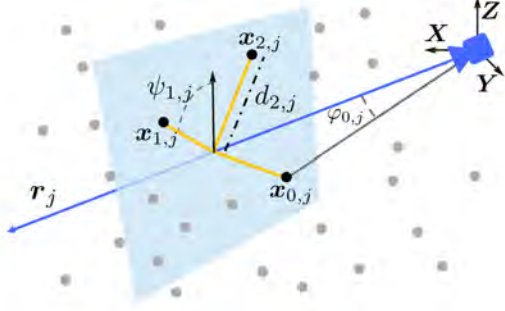


Figure 4: The ray-point distances are illustrated for a ray j and the $k = 3$ closest points. For a better visualization the ray and points are translated with $-o_j$ into the scene’s coordinate frame and all points are projected into a single plane instead of 3 parallel planes.

$T = 4$ known from NeRF [26] and further explained by Tancik et al. [45] to interpolate high frequency data from a low frequency input domain. The point latents l_k and the positional encoded distances are concatenated to a unique descriptor $v_{k,j}$ between ray r_j and point k , that encompasses the positional encoding and the latent information of that point. The descriptor $v_{k,j}$ is then passed through two MLPs with two layers that predict a key $K_{k,j}$ and value $V_{k,j}$ for each of the K point ray pairs.

$$V_{k,j} = F_{\theta_V}(v_{k,j}), K_{k,j} = F_{\theta_K}(v_{k,j}) \quad (8)$$

$$Q_j = F_{\theta_Q}(\gamma(d_j)) \quad (9)$$

From the positionally encoded ray direction $\gamma(d_j)$, we derive a query vector Q_j . The ray direction d_j is again presented in world coordinates here, such that it will produce the same result independent from any coordinate reference in the locally captured scene. The multi-head attention learns to predict a weight for all $V_{k,j}$ given $K_{k,j}$ for each selected point ray pair (k,j) and a query ray Q_j . The aggregated output of the multi-head attention module is then a latent code $l_j \in \mathcal{R}^{128}$, that describes the light fields for each ray r_j , that is

$$\text{multi-head attention: } l_j = F_{\theta_{attn}}(Q_j, K_{k,j}, V_{k,j}). \quad (10)$$

Points Beyond the Point Cloud. In most automotive datasets the captured point cloud data only captures the scene geometry from the ground plane up to a height of multiple meters. Thus there are parts of the scene which are not explicitly captured in the point cloud data, such as high building structures and the sky. We therefore set a threshold d_∞ below which we consider rays to intersect with the point cloud. The value d_∞ is chosen as the maximum distance between two points in any P_i after ignoring outlying points. Only for points that exceed d_∞ we concatenate $v_{k,j}$ with a learned global latent code l_∞ , such that the attention module can leverage both a global and point feature representation.

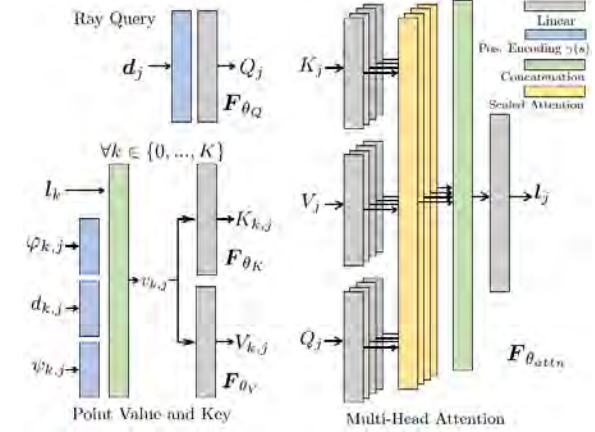


Figure 5: The multi-headed self-attention module aggregates the latent encoding l_j of ray j given the ray direction d_j from the information of the K closest points. For each point k an embedding $v_{k,j}$ is computed from the point’s feature and the positional encoded relative location to r_j for each ray-point pair (j,k) . F_{θ_K} and F_{θ_V} compute the key K and value V vectors from $v_{k,j}$. The query vector Q is predicted for the ray’s direction d_j .

The point features are still useful as they may contain relevant context and geometry for structures that rise above the point cloud.

3.3. RGB Prediction

Now that we have shown how we predict a latent vector l_j for any ray r_j from encodings on a sparse point cloud, we are finally able to reconstruct the color C_j for an arbitrary ray in our global scene, that is

$$F_{\theta_{LF}} : (d_j, j) \rightarrow C \quad (11)$$

$$C_j = F_{\theta_{LF}}(d_j \oplus l_j) \quad (12)$$

Here, given the ray direction d_j and index j , that accesses the respective latent code, we evaluate a learned color mapping function in Eq. 11, that predicts the color along each ray in the light field. Ray direction and latent vector are concatenated $(d_j \oplus l_j)$ and the mapping from the light field representation is approximated with an eight layer and 256 wide MLP, that is trained jointly with all other modules. Implementation details for this and all other modules are provided in the supplementary materials. For each predicted ray color $\hat{C}(r_j)$ we can compute the mean-squared error image loss

$$\mathcal{L} = \sum_{j \in \mathcal{R}} \|\hat{C}(r_j) - C(r_j)\|_2^2. \quad (13)$$

Training All parameters of the model, that is $\theta_{ResNet18}$, θ_K , θ_V , θ_Q , θ_{attn} and θ_{LF} , are jointly optimized using the respective gradients computed by back propagating from the presented loss in Eq. 13 to each parameter. In each step we randomly sample 8192 rays for \mathcal{R} from a small batch of frames. All parameter are trained using the Adam optimizer [18] with a linear learning rate decay.



Figure 6: Scene Reconstruction. We present results for reconstructing images for poses seen during training of NeRF [25], DS-NeRF [8], GSN [9] and Neural Point Light Fields. All methods were trained on the same set of scene of the Waymo Open Dataset [44]. NeRF, even with substantially increased model capacity, and DS-NeRF show similar blurriness and other artifacts, while the depth supervision allows DS-NeRF improve upon existing methods. GSN produces fewer artifacts, struggles to reconstruct fine details, and fails for sparsely observed views (center scene). Neural Point Light Fields most faithfully reconstructs the image from the data set, see also Tab. 2.

4. Assessment

To assess the proposed method, we evaluate its complexity and train neural point light fields on an automotive driving dataset. Specifically, we compare against state-of-the-art neural rendering methods by generating novel views interpolating between poses on the driven trajectory as well as extrapolating to completely new trajectories. Moreover, we analyze how architecture and parameter choices in the proposed method affect reconstruction quality.

4.1. Complexity

Volumetric neural rendering methods require a large number of samples per ray for accurate results. Even though existing methods allow to speed up rendering times [17], training often requires hundreds of ray samples. We report the measured time and counted evaluations for a ray evaluation during training and inference in Tab. 1. To avoid differences due to pre-caching of rays or similar speed-ups in an implementation, the evaluation time is measured after the ray sampling step for a respective PyTorch [32] implementation of the method. The measured times include the encoding and decoding steps, e.g., point encoding (ours), convolution refinement (GSN), but divided by the number of pixels in an image to compute the time per ray.

In contrast to volumetric scene representations, that need a high number of sampling points, even when supported by local latents, Neural Point Light Fields only require a single evaluation per ray during rendering. When measured, this results in two times speedup, although our method incurs overhead to extract point features.

Cost	NeRF [26]	DS-NeRF [8]	GSN [9]	Ours
No. of Evaluations	192	192	64	1
Time per ray, training (in μ s)	146	146	<u>37</u>	34
Time per ray, inference (in μ s)	49	49	<u>17</u>	10

Table 1: Complexity per ray during training and inference. All volumetric approaches require multiple evaluations per ray. Neural Point Light Fields (Ours) has a complexity of $O(1)$ per rendered ray. Despite an added complexity in the feature extraction step, this allows for shorter training and inference.

4.2. Experimental Setup

We quantitatively and qualitatively validate the proposed method on two tasks, reconstruction and novel view synthesis, where we compare against Generative Scene Networks (GSN), NeRF and depth-supervised NeRF (DS-NeRF). GSN has been successfully applied to large scale indoor scenes [9] and takes advantage of a local embedding of the scene that is jointly learned with the scene. In contrast to our sparse point features, the latent codes are located on a sparse 2D floorplan. We evaluate NeRF [26] as a state-of-the-art implicit scene representation. Additionally we evaluate DS-NeRF [8], which takes advantage of an additional depth supervision for the opacity prediction. The depth images for GSN and the per ray depth information for DS-NeRF are directly projected from the recorded point cloud data, allowing these methods to see point cloud data in addition to RGB images. All methods were trained with the code, that was published by the authors and the experimental configurations closest to the scenario of outdoor/free moving scenes. For our method we use a maximum of $N = 20000$ randomly sampled points, $K = 8$ close

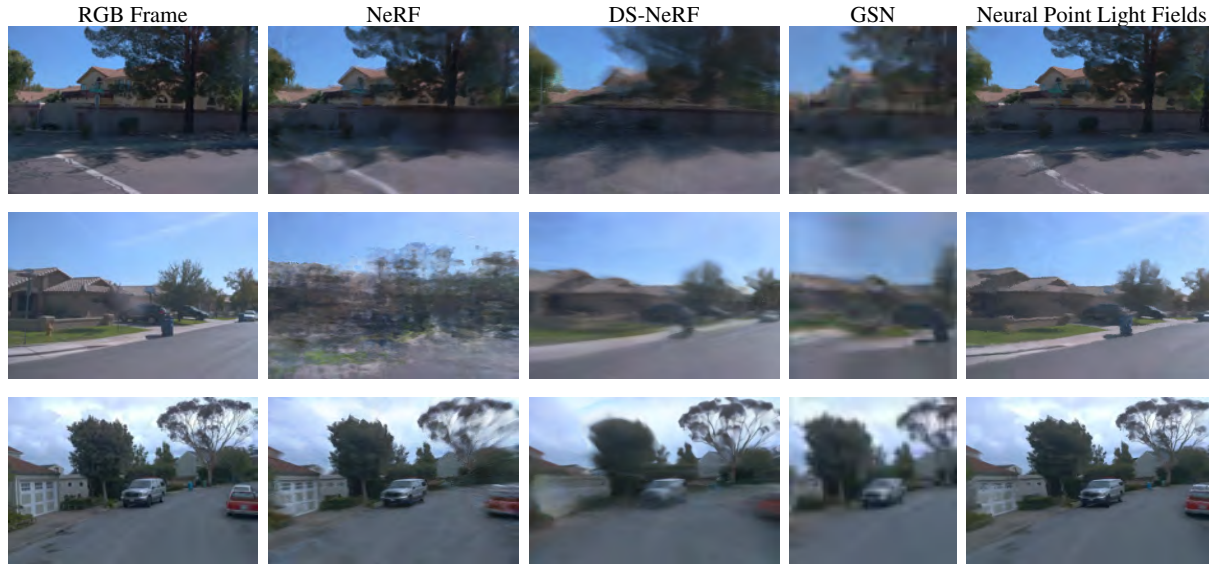


Figure 7: Novel View Interpolation. We predict views for unseen poses held-out from the training data for a scene. The images shown in the middle rows stem from the longest selected scenes (200 frames) and the other from shorter subsections (80 frames). NeRF and DS-NeRF show blurry and over smooth results, but perform better on smaller scenes. NeRF synthesizes the details on the small scenes better, while it fails completely on the larger scenes, even when substantially increasing the model capacity. GSN performs consistently across all scenes, but lacks detail and shows artifacts. Neural Point Light Fields as a representation allow for high-quality synthesis for novel view interpolation.

points, 128 dimensional point and ray embedding l_k and l_j , and 8 heads in the multi-head attention module.

All methods except GSN were trained on 6 scenes from the Waymo Open Dataset [44] with a length ≤ 200 frames, see Supplemental Document. To train on a single GPU, we downsample to the eighth of the original resolution resulting in a resolution of 240x160 pixels. For GSN, a convolutional refinement step requires the models to be trained on the full image and the code provided hard-coded settings that required us, after consulting with the authors, to crop to a square resolution of 64x64. Results on GSN are provided for 3 scenes and all metrics for GSN are calculated on down sampled images of the data set, to make the evaluation fair. Note that GSN has an advantage in all quantitative evaluations as a smaller FOV at lower resolution needs to be synthesized. All out models were trained until convergence on each scene on a mixture of NVIDIA TITAN Xp and NVIDIA V100 GPUs. Complexity evaluations were computed on the same hardware. The lower resolution requirements on GSN for over-fitting on a single scene resulted in a training time of 2 days, while the other models trained for 2 to 3 days varying with scene frame count.

Quantitative Evaluation. We evaluate the proposed method for reconstruction of seen frames, and novel view synthesis of unseen, held-out frames, where we average evaluations across all scenes. We train all methods on the same 90% of all frames of the driven trajectory. The left out 10% are used for evaluating the ability to interpolate novel views inside the seen trajectory. Tab. 2 reports quantitative

	NeRF [26]	DS-NeRF [8]	GSN [9]	Ours
Reconstruction				
PSNR \uparrow	<u>29.48</u>	26.53	17.98	31.52
SSIM \uparrow	<u>0.815</u>	0.778	0.512	0.882
LPIPS \downarrow	0.289	0.306	<u>0.136</u>	0.110
Novel View Synthesis				
PSNR \uparrow	22.47	<u>26.15</u>	16.83	29.96
SSIM \uparrow	0.700	<u>0.772</u>	0.464	0.868
LPIPS \downarrow	0.389	0.310	<u>0.174</u>	0.119

Table 2: We report PSNR, SSIM and LPIPS results on 5 static scenes from the Waymo Open Dataset [44] using images from the front camera for NeRF [26], depth-supervised NeRF [8], and generative scene networks [9] and Neural Point Light Fields. For PSNR and SSIM, higher is better; for LPIPS lower is better. The best values are written in **bold**, the next best are underlined. Our method outperforms all methods with respect to all metrics. While NeRF shows only slightly worse reconstruction performance, DS-NeRF provides better novel view synthesis capabilities.

results for both tasks with PSNR, SSIM [48] and LPIPS [52] metrics. While NeRF is close to the proposed method with respect to the PSNR metric on the reconstruction task it performs similar to DS-NeRF on the SSIM and LPIPS metric. GSN makes an overall worse impression than the other methods in both tasks. The proposed method outperforms all other methods in all metrics. While NeRF performs significantly worse in the Novel View Synthesis task DS-NeRF shows only a slightly worse performance compared to reconstruction results, probably benefiting from a better opacity prediction when trained on a sparse set of images. Our method shows the best results, with narrow margin to the

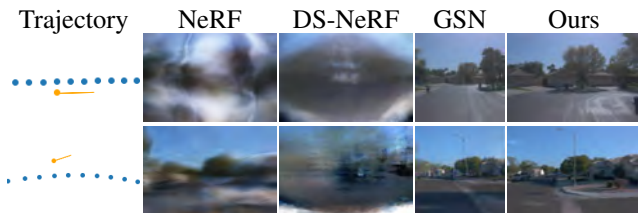


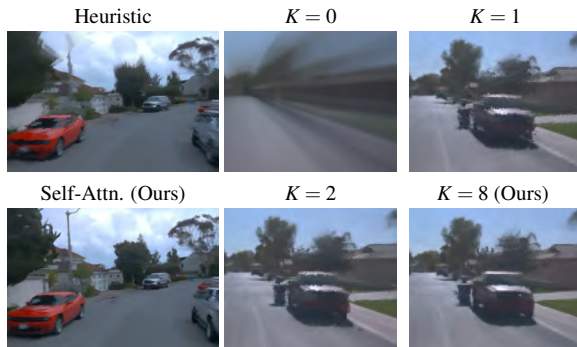
Figure 8: Novel View Trajectory Extrapolation. Extrapolating views (orange) from the training trajectory (blue). NeRF and DS-NeRF are not able to synthesize views of the scene far from the training trajectory. The proposed method achieves similar quality when compared to reconstruction and trajectory interpolation.

quality achieved by our method on the reconstruction task, in contrast to NeRFs results.

Scene Reconstruction. The results shown in Fig. 6 support the quantitative evaluation from Tab. 2. While NeRF produces inconsistent and blurry predictions for the large scenes we address in this work, it is still able to recover some details on straight scenes. We hypothesize, that the blurriness arises from the requirements of an accurate pose and the sparse set of training views on a long trajectories through a scene. DS-NeRF shows a similar behavior, but lacks some detail that has been reconstructed in NeRF and produces smooth artifacts. Renderings of the depth map of the trained scene suggest that the point cloud capture is too smooth for DS-NeRF representation and, as such, suppresses high frequency features. GSN in contrast produces an overall consistent reconstruction independent of scene length. Nevertheless results show smoothing even in the significantly down-scaled resolution that GSN accepts. In contrast, Neural Point Fields allow to reconstruct all structures independent of their position and appearance across frames. Few artifacts on very fine structures such as individual tree branches, leafs remain. Please also see the video in the Supplementary Materials.

Novel View Trajectory Interpolation. We next compare views synthesized for frames left out in the training data in Fig. 7. DS-NeRF suffers from blur and ghosting in the interpolation task. NeRF shows a similar, but less strong artifact on the few scenes that it does converge on. This stability issue for long scenes is significant, when we compare the results in the two top scenes with the two bottom scenes, that are only half as long as the two other scenes. The results validate that these existing methods are not able to effectively synthesize scenes just from a sparse set of images. GSN, that uses a local support, is more consistent resulting in similar outputs in both tasks independent of scene length. Neural Point Light Fields encode the scenes features on a sparse set of points and hence achieve high-quality novel view interpolation over long sequences.

Novel View Trajectory Extrapolation. The results shown in Fig. 8 report visual extrapolation experiments. We



	Naive Sum	Heuristic	$K = 0$	$K = 1$	$K = 2$	Ours
PSNR \uparrow	4.84	24.56	18.88	29.83	30.95	31.52

Figure 9: Ablation studies. Qualitative and quantitative results of ablations for the number of closest points K and different approaches for the light field interpolation module.

present a map of the novel views camera pose with respect to the training trajectory. Our method is able to generate a set of novel trajectories and scenes, that can hardly differentiated from the interpolation and reconstruction results. This is possible inside a certain bound of the scene at least partially covered by the training views, see Supplemental Material. Views into regions of a scene, that were not seen during training, e.g., the back of a vehicle only seen from the front result in imaginary objects from conditioned on points similar to seen objects. In the future, including additional cameras in a 360 surround view application, may allow to cover even such entirely occluded scene parts.

4.3. Ablations

Next, we analyze architecture and parameter choices in Fig. 9. The proposed self-attention to aggregate a single ray feature is crucial. We found that a heuristic weighting or a naive sum over all point features are not able to achieve similar results. While the naive sum is not able to train at all, a heuristic weighting of each point feature by the inverse distance $d_{k,j}$ achieves better results. However, this weighting still lacks detail, suffers from artifacts and noisy reconstruction of the scene. We propose to index a set of points, in contrast to methods that purely parametrize a ray. Also the decision to use a set of points is necessary to learn the light field of such a large scene, that can not be embedded solely on a single or two points. We choose $K = 0, 1, 2, 8$ to illustrate this effect in Fig. 9. Further ablation studies are provided in the Supplementary Materials.

5. Conclusion

We introduce an implicit representation that encodes a local light field on a point cloud. Departing from volumetric representations that require querying radiance estimates at hundreds of sample points along a ray cast into the volume,

we learn realistic radiance fields with only a single radiance sample per ray. Neural point light fields are functions of the ray direction, and local point feature neighborhood, which allows us to interpolate the light field conditioned training images without densely captured input views. As such, the method allows for novel view synthesis in large-scale automotive scenarios, with only a few sparse view directions available during a drive-by capture. We validate the proposed method for novel view synthesis when interpolating and extrapolating along unseen trajectories where existing implicit representation methods fail. While it is typical in automotive scenarios to have point cloud captures available, in the future, we plan to jointly recover point positions and local features of the proposed neural point light fields.

Acknowledgements

We thank ServiceNow for providing compute resources for this project with the ServiceNow Toolkit.

References

- [1] Edward H Adelson, James R Bergen, et al. *The plenoptic function and the elements of early vision*, volume 2. Vision and Modeling Group, Media Laboratory, Massachusetts Institute of . . . , 1991. [2](#)
- [2] Sameer Agarwal, Yasutaka Furukawa, Noah Snavely, Ian Simon, Brian Curless, Steven M. Seitz, and Richard Szeliski. Building rome in a day. *Commun. ACM*, 54(10):105–112, Oct 2011. [2](#)
- [3] Kara-Ali Aliev, Artem Sevastopolsky, Maria Kolos, Dmitry Ulyanov, and Victor Lempitsky. Neural point-based graphics. 2020. [3](#)
- [4] Kara-Ali Aliev, Artem Sevastopolsky, Maria Kolos, Dmitry Ulyanov, and Victor Lempitsky. Neural point-based graphics. In *Computer Vision–ECCV 2020: 16th European Conference, Glasgow, UK, August 23–28, 2020, Proceedings, Part XXII 16*, pages 696–712. Springer, 2020. [3](#)
- [5] Relja Arandjelović and Andrew Zisserman. Nerf in detail: Learning to sample for view synthesis. *arXiv preprint arXiv:2106.05264*, 2021. [3](#)
- [6] Robert C Bolles, H Harlyn Baker, and David H Marimont. Epipolar-plane image analysis: An approach to determining structure from motion. *International journal of computer vision*, 1(1):7–55, 1987. [2](#)
- [7] Mark Boss, Raphael Braun, Varun Jampani, Jonathan T Barron, Ce Liu, and Hendrik Lensch. Nerd: Neural reflectance decomposition from image collections. In *Proceedings of the IEEE/CVF International Conference on Computer Vision*, pages 12684–12694, 2021. [1](#)
- [8] Kangle Deng, Andrew Liu, Jun-Yan Zhu, and Deva Ramanan. Depth-supervised nerf: Fewer views and faster training for free. *arXiv preprint arXiv:2107.02791*, 2021. [3](#), [6](#), [7](#)
- [9] Terrance DeVries, Miguel Angel Bautista, Nitish Srivastava, Graham W Taylor, and Joshua M Susskind. Unconstrained scene generation with locally conditioned radiance fields. *arXiv preprint arXiv:2104.00670*, 2021. [4](#), [6](#), [7](#)
- [10] John Flynn, Michael Broxton, Paul Debevec, Matthew DuVall, Graham Fyffe, Ryan Overbeck, Noah Snavely, and Richard Tucker. Deepview: View synthesis with learned gradient descent. *Proceedings IEEE/CVF Conference on Computer Vision and Pattern Recognition (CVPR)*, Jun 2019. [3](#)
- [11] Stephan J Garbin, Marek Kowalski, Matthew Johnson, Jamie Shotton, and Julien Valentin. Fastnerf: High-fidelity neural rendering at 200fps. *arXiv preprint arXiv:2103.10380*, 2021. [3](#)
- [12] Andreas Geiger, Philip Lenz, and Raquel Urtasun. Are we ready for autonomous driving? the kitti vision benchmark suite. In *Proceedings of the IEEE Conference on Computer Vision and Pattern Recognition (CVPR)*, 2012. [2](#), [3](#)
- [13] Ankit Goyal, Hei Law, Bowei Liu, Alejandro Newell, and Jia Deng. Revisiting point cloud shape classification with a simple and effective baseline. *arXiv preprint arXiv:2106.05304*, 2021. [2](#), [3](#)
- [14] Abdullah Hamdi, Silvio Giancola, and Bernard Ghanem. Mvtn: Multi-view transformation network for 3d shape recognition. In *Proceedings of the IEEE/CVF International Conference on Computer Vision*, pages 1–11, 2021. [3](#)
- [15] Zekun Hao, Arun Mallya, Serge Belongie, and Ming-Yu Liu. Gancraft: Unsupervised 3d neural rendering of minecraft worlds. *arXiv preprint arXiv:2104.07659*, 2021. [1](#)
- [16] Kaiming He, Xiangyu Zhang, Shaoqing Ren, and Jian Sun. Deep residual learning for image recognition. In *Proceedings of the IEEE conference on computer vision and pattern recognition*, pages 770–778, 2016. [3](#)
- [17] Peter Hedman, Pratul P Srinivasan, Ben Mildenhall, Jonathan T Barron, and Paul Debevec. Baking neural radiance fields for real-time view synthesis. *arXiv preprint arXiv:2103.14645*, 2021. [1](#), [6](#)
- [18] Diederik P. Kingma and Jimmy Ba. Adam: A method for stochastic optimization. *CoRR*, abs/1412.6980, 2015. [5](#)
- [19] Georgios Kopanas, Julien Philip, Thomas Leimkühler, and George Drettakis. Point-based neural rendering with per-view optimization. In *Computer Graphics Forum*, volume 40, pages 29–43. Wiley Online Library, 2021. [1](#), [3](#)
- [20] Marc Levoy and Pat Hanrahan. Light field rendering. In *Proceedings of the 23rd annual conference on Computer graphics and interactive techniques*, pages 31–42, 1996. [2](#)
- [21] Lingjie Liu, Jiatao Gu, Kyaw Zaw Lin, Tat-Seng Chua, and Christian Theobalt. Neural sparse voxel fields. *arXiv preprint arXiv:2007.11571*, 2020. [1](#), [3](#)
- [22] Stephen Lombardi, Tomas Simon, Jason Saragih, Gabriel Schwartz, Andreas Lehrmann, and Yaser Sheikh. Neural volumes: Learning dynamic renderable volumes from images. *ACM Trans. Graph.*, 38(4):65:1–65:14, Jul 2019. [1](#), [2](#)
- [23] Erika Lu, Forrester Cole, Tali Dekel, Weidi Xie, Andrew Zisserman, David Salesin, William T. Freeman, and Michael Rubinstein. Layered neural rendering for retiming people in video, 2020. [3](#)
- [24] Ricardo Martin-Brualla, Noha Radwan, Mehdi S. M. Sajjadi, Jonathan T. Barron, Alexey Dosovitskiy, and Daniel Duckworth. NeRF in the Wild: Neural Radiance Fields for Unconstrained Photo Collections. In *arXiv*, 2020. [3](#)

- [25] Ben Mildenhall, Pratul P. Srinivasan, Rodrigo Ortiz-Cayon, Nima Khademi Kalantari, Ravi Ramamoorthi, Ren Ng, and Abhishek Kar. Local light field fusion: Practical view synthesis with prescriptive sampling guidelines. *ACM Transactions on Graphics (TOG)*, 2019. 2, 3, 6
- [26] Ben Mildenhall, Pratul P. Srinivasan, Matthew Tancik, Jonathan T. Barron, Ravi Ramamoorthi, and Ren Ng. Nerf: Representing scenes as neural radiance fields for view synthesis, 2020. 1, 3, 5, 6, 7
- [27] Thomas Neff, Pascal Stadlbauer, Mathias Parger, Andreas Kurz, Chakravarty R Alla Chaitanya, Anton Kaplanyan, and Markus Steinberger. Donerf: Towards real-time rendering of neural radiance fields using depth oracle networks. 40, 2021. 3
- [28] Michael Niemeyer and Andreas Geiger. Giraffe: Representing scenes as compositional generative neural feature fields. In *Proc. IEEE Conf. on Computer Vision and Pattern Recognition (CVPR)*, 2021. 3
- [29] Michael Niemeyer, Lars Mescheder, Michael Oechsle, and Andreas Geiger. Differentiable volumetric rendering: Learning implicit 3d representations without 3d supervision. In *Proceedings of the IEEE Conference on Computer Vision and Pattern Recognition (CVPR)*, 2020. 1, 2
- [30] Julian Ost, Fahim Mannan, Nils Thuerey, Julian Knodt, and Felix Heide. Neural scene graphs for dynamic scenes. In *Proceedings of the IEEE/CVF Conference on Computer Vision and Pattern Recognition (CVPR)*, pages 2856–2865, 2021. 3
- [31] Keunhong Park, Utkarsh Sinha, Jonathan T. Barron, Sofien Bouaziz, Dan B Goldman, Steven M. Seitz, and Ricardo Martin-Brualla. Nerfies: Deformable neural radiance fields. *Proceedings of the IEEE International Conference on Computer Vision*, 2021. 3
- [32] Adam Paszke, Sam Gross, Francisco Massa, Adam Lerer, James Bradbury, Gregory Chanan, Trevor Killeen, Zeming Lin, Natalia Gimelshein, Luca Antiga, Alban Desmaison, Andreas Kopf, Edward Yang, Zachary DeVito, Martin Raison, Alykhan Tejani, Sasank Chilamkurthy, Benoit Steiner, Lu Fang, Junjie Bai, and Soumith Chintala. Pytorch: An imperative style, high-performance deep learning library. In H. Wallach, H. Larochelle, A. Beygelzimer, F. d'Alché-Buc, E. Fox, and R. Garnett, editors, *Advances in Neural Information Processing Systems 32*, pages 8024–8035. Curran Associates, Inc., 2019. 6
- [33] Francesco Pittaluga, Sanjeev J Koppal, Sing Bing Kang, and Sudipta N Sinha. Revealing scenes by inverting structure from motion reconstructions. In *Proceedings of the IEEE Conference on Computer Vision and Pattern Recognition (CVPR)*, pages 145–154, 2019. 3
- [34] Charles R Qi, Hao Su, Kaichun Mo, and Leonidas J Guibas. Pointnet: Deep learning on point sets for 3d classification and segmentation. In *Proceedings of the IEEE/CVF Conference on Computer Vision and Pattern Recognition (CVPR)*, pages 652–660, 2017. 3
- [35] Gernot Riegler and Vladlen Koltun. Free view synthesis. In *European Conference on Computer Vision*, pages 623–640. Springer, 2020. 1, 3
- [36] Gernot Riegler and Vladlen Koltun. Stable view synthesis. In *Proceedings of the IEEE/CVF Conference on Computer Vision and Pattern Recognition*, pages 12216–12225, 2021. 1, 3
- [37] Johannes Lutz Schönberger and Jan-Michael Frahm. Structure-from-Motion Revisited. In *Proceedings of the IEEE Conference on Computer Vision and Pattern Recognition (CVPR)*, 2016. 3
- [38] Johannes Lutz Schönberger, Enliang Zheng, Marc Pollefeys, and Jan-Michael Frahm. Pixelwise View Selection for Unstructured Multi-View Stereo. In *Proceedings of the IEEE European Conf. on Computer Vision (ECCV)*, 2016. 2, 3
- [39] Katja Schwarz, Yiyi Liao, Michael Niemeyer, and Andreas Geiger. Graf: Generative radiance fields for 3d-aware image synthesis. In *Advances in Neural Information Processing Systems (NeurIPS)*, 2020. 3
- [40] Vincent Sitzmann, Justus Thies, Felix Heide, Matthias Nießner, Gordon Wetzstein, and Michael Zollhöfer. Deepvoxels: Learning persistent 3d feature embeddings. In *Proceedings of the IEEE/CVF Conference on Computer Vision and Pattern Recognition (CVPR)*, 2019. 3
- [41] Vincent Sitzmann, Michael Zollhöfer, and Gordon Wetzstein. Scene representation networks: Continuous 3d-structure-aware neural scene representations. In *Advances in Neural Information Processing Systems*, 2019. 1
- [42] Pratul P Srinivasan, Boyang Deng, Xiuming Zhang, Matthew Tancik, Ben Mildenhall, and Jonathan T Barron. Nerv: Neural reflectance and visibility fields for relighting and view synthesis. In *Proceedings of the IEEE/CVF Conference on Computer Vision and Pattern Recognition (CVPR)*, pages 7495–7504, 2021. 1, 3
- [43] P. P. Srinivasan, R. Tucker, J. T. Barron, R. Ramamoorthi, R. Ng, and N. Snavely. Pushing the boundaries of view extrapolation with multiplane images. In *Proceedings of the IEEE/CVF Conference on Computer Vision and Pattern Recognition (CVPR)*, pages 175–184, 2019. 3
- [44] Pei Sun, Henrik Kretzschmar, Xerxes Dotiwalla, Aurelien Chouard, Vijaysai Patnaik, Paul Tsui, James Guo, Yin Zhou, Yuning Chai, Benjamin Caine, et al. Scalability in perception for autonomous driving: Waymo open dataset. In *Proceedings of the IEEE/CVF Conference on Computer Vision and Pattern Recognition (CVPR)*, pages 2446–2454, 2020. 2, 6, 7
- [45] Matthew Tancik, Pratul P. Srinivasan, Ben Mildenhall, Sara Fridovich-Keil, Nithin Raghavan, Utkarsh Singhal, Ravi Ramamoorthi, Jonathan T. Barron, and Ren Ng. Fourier features let networks learn high frequency functions in low dimensional domains, 2020. 5
- [46] Justus Thies, Michael Zollhöfer, and Matthias Nießner. Deferred neural rendering. *ACM Transactions on Graphics*, 38(4):1–12, Jul 2019. 3
- [47] Ashish Vaswani, Noam Shazeer, Niki Parmar, Jakob Uszkoreit, Llion Jones, Aidan N Gomez, Łukasz Kaiser, and Illia Polosukhin. Attention is all you need. In *Advances in neural information processing systems*, pages 5998–6008, 2017. 4
- [48] Z. Wang, Eero Simoncelli, and Alan Bovik. Multiscale structural similarity for image quality assessment. volume 2, pages 1398 – 1402 Vol.2, 12 2003. 7

- [49] Sven Wanner and Bastian Goldluecke. Globally consistent depth labeling of 4d light fields. In *2012 IEEE Conference on Computer Vision and Pattern Recognition*, pages 41–48. IEEE, 2012. 2
- [50] Sven Wanner and Bastian Goldluecke. Variational light field analysis for disparity estimation and super-resolution. *IEEE transactions on pattern analysis and machine intelligence*, 36(3):606–619, 2013. 2
- [51] Wenqi Xian, Jia-Bin Huang, Johannes Kopf, and Changil Kim. Space-time neural irradiance fields for free-viewpoint video. In *Proceedings of the IEEE/CVF Conference on Computer Vision and Pattern Recognition (CVPR)*, pages 9421–9431, 2021. 3
- [52] Richard Zhang, Phillip Isola, Alexei A Efros, Eli Shechtman, and Oliver Wang. The unreasonable effectiveness of deep features as a perceptual metric. In *Proceedings of the IEEE conference on computer vision and pattern recognition (CVPR)*, pages 586–595, 2018. 7
- [53] Xiuming Zhang, Pratul P Srinivasan, Boyang Deng, Paul Debevec, William T Freeman, and Jonathan T Barron. Nerfactor: Neural factorization of shape and reflectance under an unknown illumination. *arXiv preprint arXiv:2106.01970*, 2021. 1
- [54] Tinghui Zhou, Richard Tucker, John Flynn, Graham Fyffe, and Noah Snavely. Stereo magnification: Learning view synthesis using multiplane images. In *SIGGRAPH*, 2018. 3